Time-Variable Gravity: Using Satellite Laser Ranging as a Tool for Observing Long-Term Changes in the Earth System

Christopher Cox[1,3], Andrew Au[1,3], Jean-Paul Boy[2,3], Benjamin Chao[3]
[1]Raytheon ITSS, Lanham, MD, USA
[2]University of Maryland Baltimore County, Baltimore, MD, USA
[3]Space Geodesy Branch, NASA Goddard Space Flight Center, Greenbelt, MD, USA

Abstract

Temporal variations in the long-wavelength gravity field have been observed using the satellite-laser-ranging (SLR) technique for the past twenty years. The long-term trends in these estimates have generally been consistent with and attributable to post glacial rebound, in addition to a number of secondary contributors. However, since 1998, the Earth's oblateness parameter J_2 reversed its decreasing trend and began increasing. At present we don't have strong indications whether this aberration represents a change in the long-term rate, or whether it is short term in nature. In addition to changes in the mean J_2, the amplitude of the annual variation has been changing. This change signifies a large change in global mass distribution whose J_2 effect clearly overshadows that of the post-glacial rebound. A number of possible causes have been considered, with oceanic mass redistribution as the leading candidate and core effects as another possible alternative. Several components of the low-degree time series show correlation to known ocean processes. These include correlations between the sectorials and the Southern Oscillation Index, as well as some level of long-term correlation between the Pacific Decadal Oscillation and the observed J_2 series. While the exact cause of the recent changes in J_2 may not have been formally identified, these results do indicate the usefulness of SLR as a tool to observe long-term changes in the climate. We will present our analysis of the changes in the low-degree spherical harmonics of the gravity field and results of our investigations into the causes.

Introduction

The long time history of satellite laser ranging (SLR) provides an absolutely unique data set of observations for the analysis of geophysical changes. Analysis of SLR tracking has yielded precise determination of the temporal variation in the low-degree spherical-harmonic components of Earth's gravity field, beginning with the initial observations of J_2 change made by observing LAGEOS-1 orbital node accelerations [*Yoder et al*., 1983, and *Rubincam*, 1984]. Those earliest results demonstrated the ability to observe terrestrial change over long scales using SLR. More recent studies have extended the knowledge to higher degree zonals [e.g., *Gegout and Cazenave*, 1993, *Cheng et al*., 1997, and *Cox et al.,* 2002], and examined the annual signals in the low-degree geopotential, the non-tidal part of which is dominated by climatological signals. Overall, SLR data have played a key role in understanding changes in the solid Earth at millennial and decadal time scales, as well as providing insight into climatological variations over annual time-scales.

Zonal Rate Solutions

Table 1 shows the results of several recent zonal rate solutions. The block of results labeled "GGG2000" correspond to those described in *Cox et al*., [2002]. Agreement with the other studies is generally good, but there are sign differences in $\dot{J}_4$ and $\dot{J}_6$. For solutions that did not estimate a single odd-zonal rate, a nominal lumped coefficient is shown that is based on the lumping equation for $\dot{J}_3$ and $\dot{J}_5$. There is good agreement between the

GGG2000 results and the lumped odd-zonal rate implied by *Cheng et al.* [1997] although there is some difference in the separation of the odd-zonal rates. Comparison of the zonal rates with geophysical models has yielded fairly consistent estimates for lower mantle viscosity and ice mass balance [*Cox et al*, 2002]. So, it is fair to state that there has been reasonably good agreement between the different studies in terms of J_2 and J_{ODD} values up until the recent times.

As with the J_2 and J_{ODD} rates, the agreement between the various estimates of the 18.6-year lunar ocean tide is also reasonable. The ratio between the recovered 18.6-year lunar ocean tide in-phase amplitude (1.41 cm) from the GGG2000 base solution and the equilibrium value (1.22 cm) is about 1.16, which is close to the results of *Trupin and Wahr* [1990], who found a ratio of 1.13±0.22. There is also reasonable agreement between the simultaneously recovered 18.6-year tide amplitudes and the results of *Cheng et al.* [1997]. The 9.3-year lunar ocean tide amplitude was consistently around 0.8±0.3 mm, somewhat larger than the equilibrium value of 0.12 mm.

The block of results labeled "EGS2001" (originally presented at the 2001 EGS meeting in Nice) shows the effect of the addition of the more recent data. There is significant deviation in these solutions from the rates derived using data through 1997. Even if the assumption of no phase lag (which effectively neglects the effects of anelasticity) for the 18.6-year ocean tide is not ideal, the results in the table show that there is a significant change in both the 18.6-year tide in-phase amplitude and the estimated zonal rates when the post-1997 data are included. If J_2 is essentially linear in behavior over interannual to decadal periods, and the 18.6-year tide remains constant (in terms of amplitude and phase, as it should), then the addition of even two years of the later data should not cause such large changes. These changes prompted a more detailed assessment of the recent changes in the J_2 zonal harmonic, resulting in the study by *Cox and Chao* [2002].

Estimation of the Time Series

The *Cox and Chao* [2002] results were based on SLR data from a total of ten different satellites, covering the period from 1979 up to 2002, and has since been extended through May of 2002. Figure 1 shows a timeline of the data included by satellite. Gaps and breaks in the data sets for each spacecraft are not indicated. Data for Starlette prior to 1984 are sparse, and there are several large gaps in that record. The LAGEOS-1 data for 1979 and most of the 1980's were drawn from archives within the Space Geodesy Branch of NASA GSFC. All other data was drawn from the CDDIS servers. More data were available for the two Etalon satellites, however it was not used here. The contribution of Etalon is minimal at best, and time/cost considerations precluded the reprocessing of those data sets to match the time periods used for the other spacecraft.

Table 1. Zonal gravity rate and long period tide solutions. All zonal rate values are x10^{-11}.

Study	$\dot{J}_2$	$\dot{J}_{ODD}$	$\dot{J}_3$	$\dot{J}_4$	$\dot{J}_5$	$\dot{J}_6$	18.6-yr Tide $C_{2,0}$ Amp. (cm)
Cheng et al. [1989]	-2.5±0.3	1.2	-0.1±0.3	0.3±0.6	1.5±1.5		
Nerem and Klosko [1996]	-2.8±0.3	1.6±0.4		0.2±1.5			
Cheng et al. [1997]	-2.7±0.4	0.5	-1.3±0.5	-1.4±1.0	2.1±0.6	0.3±0.7	1.56±0.2
From GGG2000:							
Base - Data through 1997	-3.0±0.4	0.3	-0.9±0.4	1.4±1.0	1.3±0.4	-1.0±0.6	1.41±0.07
Use only LAGEOS-1, Starlette, and Ajisai	-2.7±0.5	0.1	-0.9±0.5	0.1±1.6	1.2±0.5	-0.5±0.9	1.44±0.08
Upweight LAGEOS-1 2x	-3.1±0.5	0.3	-0.8±0.2	1.2±1.0	1.3±0.3	-0.8±0.5	1.51±0.06
Assume 2 m SLR weight	-2.0±0.3	0.9	-0.8±0.3	-2.7±1.0	1.9±0.4	1.2±0.7	1.54±0.09
Estimate only $\dot{J}_2$ - $\dot{J}_5$	-2.4±0.2	0.2	-0.9±0.4	0.1±0.6	1.3±0.4		1.41±0.07
Estimate only $\dot{J}_2$ - $\dot{J}_4$	-2.5±0.2	0.3±0.1		0.3±0.6			1.43±0.07
From EGS2001:							
Revised Base – Data through 1997	*-3.0±0.3*	*0.2*	*-0.5±0.4*	*1.6±0.8*	*0.8±0.4*	*-1.0±0.5*	*1.41±0.07*
+1998-1999	-0.9±0.3	0.5	1.1±0.4	-0.5±0.9	-0.7±0.4	-1.0±0.5	0.82±0.06
+2000	-0.6±0.5	0.5	1.8±0.5	-2.2±0.6	-1.4±0.4	0.2±0.5	0.85±0.06
+1998-2000	-0.2±0.3	0.7	2.6±0.4	-2.4±0.6	-2.3±0.4	0.0±0.5	0.77±0.05
+1998-2000	-1.0±0.3	0.7	2.6±0.4	-2.4±0.6	-1.5±0.4	-0.2±0.5	Fixed @ 1.22

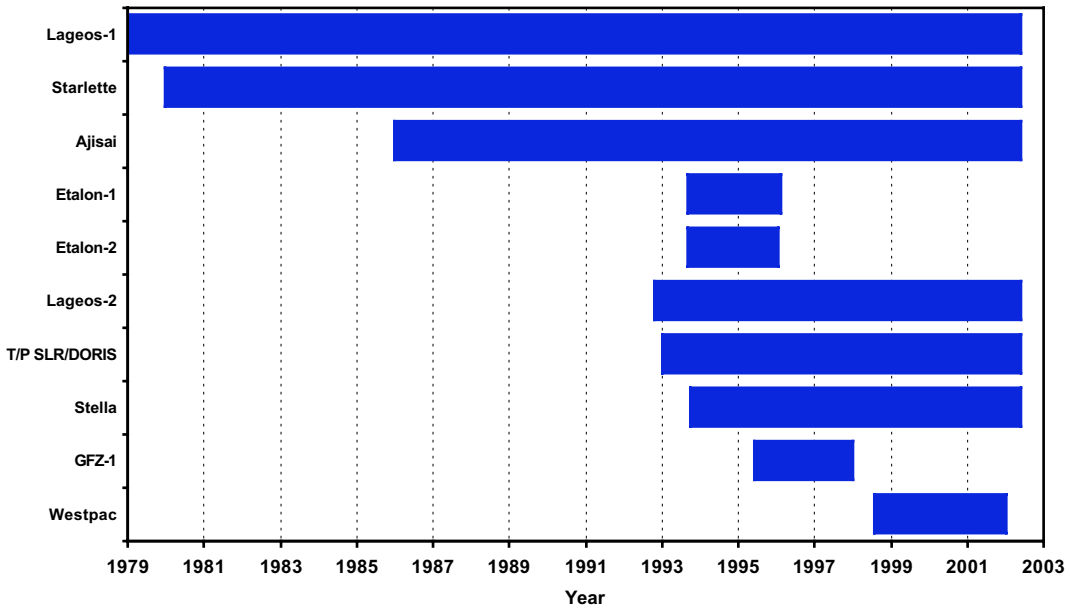

Figure 1. Time line of SLR tracking observations used to generate the low-degree geopotential series.

The SLR orbit reduction used the same station set as used in the TOPEX/Poseidon (T/P) precision orbit generation, with the addition of earlier stations for the pre-T/P data and occupations. Range biases were estimated for each station, per satellite, every ten days. This was necessary in the earlier periods where the center of mass correction applied in the data, along with other measurement corrections, could not be replaced. For consistency throughout the data series, the biases were estimated in the data reduction, but then held fixed to those values in the gravity solutions. Table 2 shows the satellites used and the general makeup of the individual satellite orbit solutions. All normal equations were generated using EGM96 [*Lemoine et al.*, 1996] as the *a priori* geopotential, and all

gravity rate partial derivatives were generated with respect to the zonal rates (and Epoch=1986.0) adopted for that model. The solid Earth tides likewise are the same as used in EGM96 and are described in more detail by *Lemoine et al*. [1998]. The ocean tide model incorporated the estimated tidal terms from EGM96, with the *Schrama and Ray* [1994] tide model as a background. The 18.6-year and 9.3-year period equilibrium Lunar tides, with zero phase lag, were also used in the SLR data. In several cases 1-cycle-per-revolution (1-CPR) accelerations were used in the data reduction to facilitate the data cleanup, however these parameters were set to 0 in the gravity solutions. In many cases exceptions to the parameterization were made in order to accommodate sparse data.

Table 2. Satellites Solutions for the SLR Data Reduction.

Satellite	*a* (km)	e	*i* (deg)	Arc Lengths	Comments
Ajisai	7870	0.001	50.0	15 days pre '92 10 days '92+	Anisotrpoic Reflectivity and Yarkovsky-Schach effects modeled 12 hour C_D (where sufficient data was present) C_R estimated per arc
Etalon-1	25501	0.001	64.9	30 days	Weak contributor
Etalon-2	25501	0.001	65.5	30 days	Weak contributor
GFZ-1	6763	0.001	51.6	10 days	~18 hour Cd (where sufficient data was present) Estimation periods broken at orbit midnight
LAGEOS-1	12273	0.005	109.9	30 days	C_R estimated every 5 days Constant Along-Track accelration every 10 days
LAGEOS-2	12163	0.013	52.6	30 days	C_R estimated every 5 days Constant Along-Track accelration every 10 days
Starlette	7331	0.021	49.8	15 days pre '92 10 days '92+	12 hour C_D (where sufficient data was present) C_R estimated per arc
Stella	7173	0.001	98.6	10 days	12 hour C_D (where sufficient data was present) C_R estimated per arc 1-CPR accelerations estimated every 5 days
T/P	7716	0.000	66.0	10 days	SLR /DORIS relative weights per precision orbits 8 hour C_D (where sufficient data was present) 1-CPR accelerations estimated every 5 days
Westpac	7173	0.001	98.6	10 days	12 hour C_D (where sufficient data was present) C_R estimated per arc 1-CPR accelerations estimated every 5 days

In all cases except GFZ-1, the high rate drag terms were held fixed to the reduction solution values in the gravity solutions. To accommodate long-wavelength along-track force model changes within the gravity solutions for those cases, constant along-track accelerations were estimated every five days. This was necessitated by periods of sparse data, the influence of the additional estimated parameters in the linearized gravity solutions, and the need to maintain consistent treatment through the gravity solution time series.

The gravity time series itself was estimated as a series of independent solutions for the geopotential complete for spherical harmonic degrees 2 through 4. The solutions periods were 90 days in 1979, 60 days from 1980 through 1991, and 30 days from 1992 onward. Each solution was formed by aggregating the satellite normal equations within the period of the solution. At this stage of the processing, the Sa and Ssa tides were set to the nominal equilibrium values. Likewise the 18.6-year and 9.3-year ocean tides were set to the values from the "Base - Data through 1997" solution shown in Table 1. Unconstrained test solutions had high noise and correlation in the non-zonals, so the solutions were constrained to the EGM96 values using a weight of 3x the standard deviation of the non-IB atmospheric gravity series. This was found to have virtually no effect on the zonals, which were well

determined, but to allow some variation in the sectorals and tesserals, without allowing a lot of noise in those parameters.

Analysis of the J_2 signal

Figure 2 shows the complete J_2 data series after removal of the atmospheric and residual annual signals. With the exception of the additional data in 2002, it is similar to Figure 2 of *Cox and Chao* [2002]. In addition to the J_2 zonal, time series for J_3 was also estimated. The J_3 zonal, which describes north-south mass distribution, does not show any significant anomalies corresponding to the timing of the J_2 event. Provided this result is accurate, it implies that whatever is causing the J_2 anomaly is largely symmetric around the Equator.

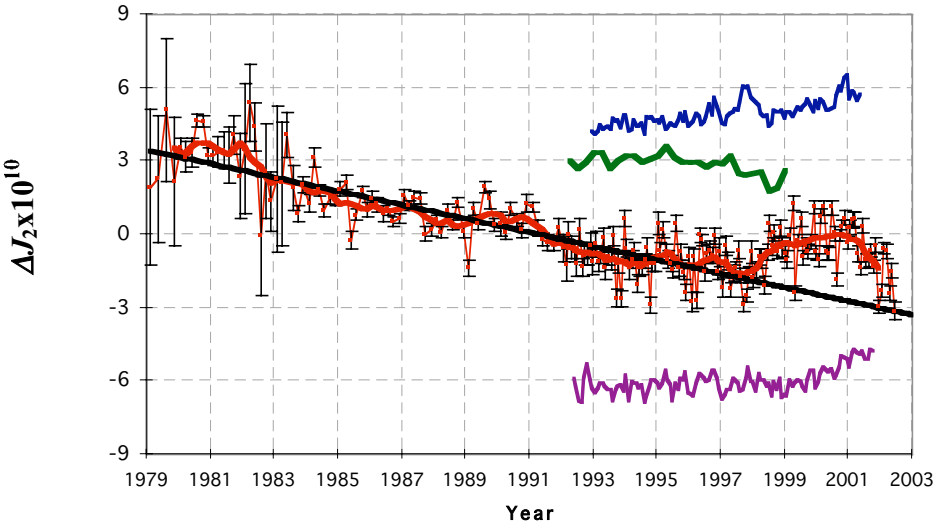

Figure 2. Observed ΔJ_2, after subtraction of the IB corrected atmospheric signal and an empirical annual term, before (thin red line with error bars) and after an annual filter has been applied (heavy red line). Error bars are the observed J_2, uncertainties. The heavy black line is a weighted fit to the (unfiltered) pre-1997 data. The slope is -2.8×10^{-11} year^{-1}. The offset green line (second from top) is the J_2 implied by the Greenland + W. Antarctic ice heights derived from ERS-1/2 altimetry data. Also shown are the J_2 implied by the T/P uniform GSL change (blue, offset, top), and that considering the geographic distribution of the sea height changes (purple, offset, bottom). Neither sea height derived estimate includes steric effects. Sampling intervals are 90 days in 1979, 60 days from 1980 through 1991, and 30 days afterwards. No detrending of rates has been performed. Units are 10^{-10}.

The atmospheric gravity correction applied to the data in Figure 2 was computed from the monthly NCEP reanalysis pressure grids assuming a two-dimensional approximation. While the atmosphere explains a good portion of the variation from the monthly to annual periods, it does not explain the anomaly. Consideration has been given to the effects of the two-dimensional "thin layer" assumptions. In this case the maximum difference between the two-dimensional and three-dimensional computations amounts to $\sim 0.5 \times 10^{-10}$ change in the annual amplitude, with no significant effect on the interannual variation.

Several other possible causes for the J_2 anomaly have been investigated, including the cryosphere, reservoirs, core, and oceans. A reasonable first guess as to the cause is accelerated melting of ice mass. The melt water must be transported from the high latitude regions to the equator to produce an effect such as the J_2 anomaly. As a hypothetical example of the magnitude of the event, Greenland would have to shed about 400 Gt of ice mass annually, with a net *additional* global sea level (GSL) rate of >1 mm/yr. However, Greenland and West Antarctica radar altimeter derived ice height changes for the 1992-1998 period show an equivalent GSL change of -0.22 mm/yr for Greenland, and -0.08 mm/yr for West Antarctica (based on preliminary results provided by J. Zwally of NASA GSFC and described in *Zwally and Brenner*, [2001]). The green curve in Figure 2 shows the implied J_2 change

caused by the ice height changes in Greenland and West Antarctica. East Antarctica, while generally considered to be in mass balance, is an unknown, but it would need to contribute ~1-2 mm/yr to GSL, depending on the scenario. Using relations based on the *Meier* [1984] estimates, mountain glaciers have a smaller effect on J_2 per unit mass than Greenland. The mass loss required to explain the observed J_2 changes would result a sea level contribution of ~2 mm/yr over the pre-1998 rate. All of these accelerated ice melt scenarios require huge GSL changes that simply have not been seen in the T/P GSL data from the NASA Ocean Altimeter Pathfinder Project. If the ice melt is going into the oceans, it must be accompanied by a significant cooling event in order to conserve GSL. Also, there is the remote possibility that the residual melt water is accumulating on land. In any case, the turnaround of the J_2 anomaly in 2001 would then imply an ice mass accumulation.

Terrestrial water impoundment is another possible factor. Large dams can individually cause a jump of $\sim 0.2 \times 10^{-10}$ in J_2, however, the cumulative effect since 1998 is far too small to explain the observed J_2 changes [*Chao*, 1995]. Regrettably there is insufficient reliable data at the moment to make reliable assessments about the role of land hydrology.

Changes in the Earth's mantle – specifically post-glacial rebound – result in the largest known interannual variation in the low degree gravity field. Such changes in the mantle occur over very long time constants due to the viscosities involved, so a mantle-originating cause for the post 1998 J_2 changes is unlikely. A more dynamic source of solid Earth variation is the core, which has generally been assumed to not be a contributor to gravity field changes. *Chao and Kuang* [2002; also W. Kuang, *private communication*, 2002], reviewed the MoSST geodynamo models [*Kuang and Chao*, 2002] and found that under some assumptions rates as large as $\sim 0.5\text{-}1.0 \times 10^{-11}$ per year due to core mass flow are possible. While the core signal may be larger than previously assumed, it still does not explain the observed J_2 anomaly.

The Contribution of the Ocean

The timing of the J_2 anomaly onset corresponds to the last big El Niño event, raising the possibility of an oceanographic connection. If the T/P Sea Surface Height (SSH) data is treated as being entirely caused by mass redistribution, the implied change in J_2 is consistent with the SLR results, if not a close match. A large uncertainty exists when interpreting the mass redistribution implications of the SSH data, because thermally driven changes in sea level have no gravity signal. Figure 3 shows the primary mode of an EOF/PC analysis of the Sea Surface Temperature (SST) and T/P SSH for the extratropic regions of the Pacific. Both the SST and SSH modes show a change around 1998. A breakdown of the SSH analysis for each region (not shown) indicates that the Northern Pacific is the dominant contributor. The SST mode corresponds to the Pacific Decadal Oscillation (PDO), which is correlated at some level with the observed J_2 data [*Cazenave and Nerem*, 2002]. The implied gravity change associated with the SSH mode is several times too small to explain the observed change in J_2, but it is symmetric about the Equator, satisfying the J_3 constraint.

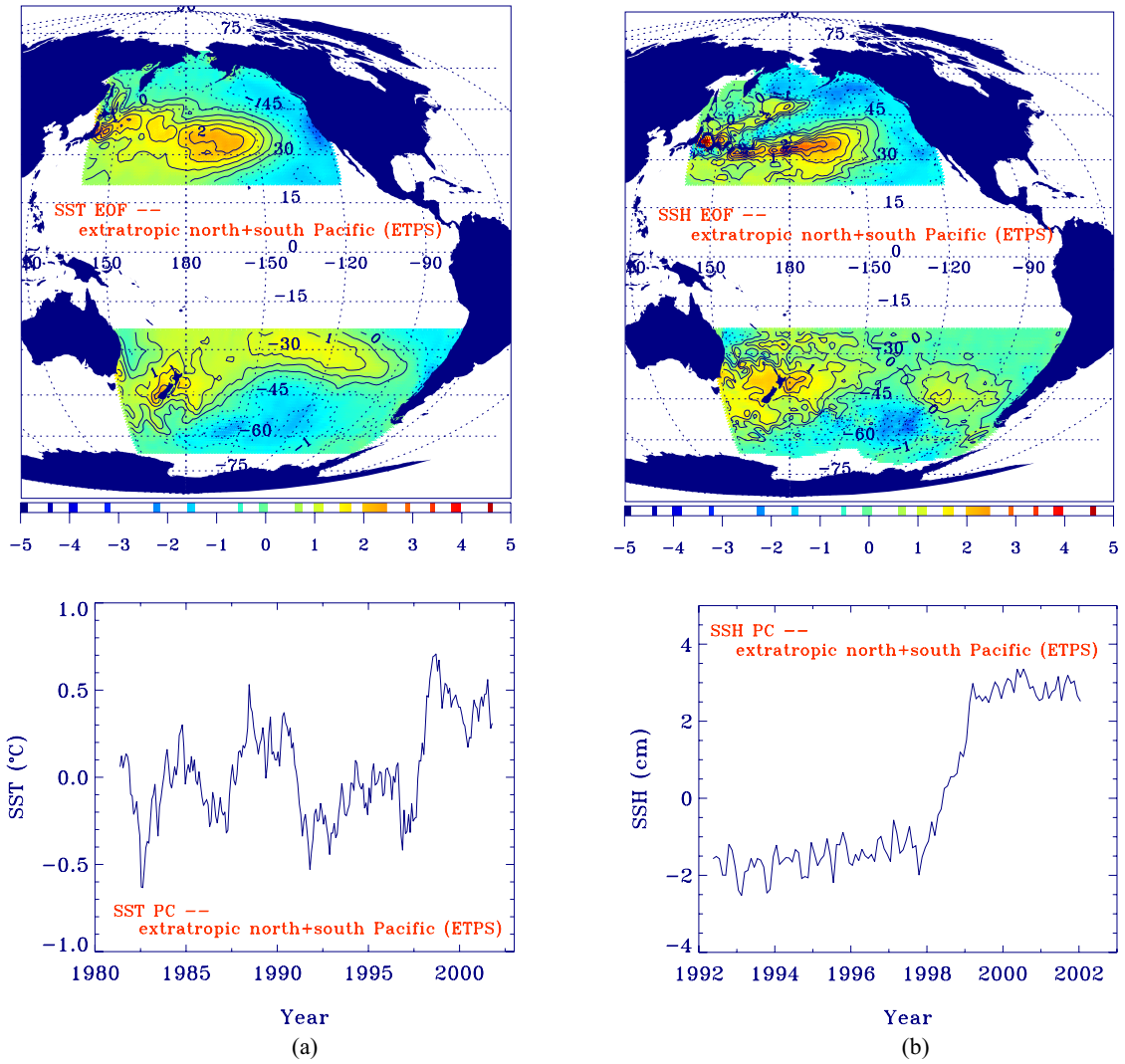

Figure 3. Primary modes of EOF/PC analyses of the (a) Sea Surface Temperature and (b) Sea Surface Height for the extratropic regions of the Pacific Ocean. The SST data series runs from 1980 through 2001, while the SSH series begins in 1992.

Initial study of the assimilation mode output of the ECCO consortium ocean model [*Stammer et al.*, 1999] shows a mass redistribution that corresponds closely in timing to the EOF/PC analyses of the T/P SSH data. Plotted in Figure 4 is the change in J_2 predicted by the ECCO model. Analysis of the EOF/PC modes of the bottom pressure shows structures corresponding to the T/P SSH and the SST observations. Similar analyses have also been performed for the Indian Ocean, North Atlantic, and South Atlantic. The dominant contributor of the five regions to J_2 is the primary mode for the Southern Pacific, with some small change in slope or offset occurring in the rest of the regions. The net jump in J_2 predicted by the ECCO assimilation model is ~0.7×10^{-10}, or only about 25% of the observed anomaly.

The correspondence between both the observational SSH and SST data and the ECCO model modes with the J_2 anomaly, as well as the correlation with PDO, supports the hypothesis of a connection with oceanic processes. However, some other source of mass redistribution (possibly driven or related to the ocean changes), or a more accurate accounting, is required to fully explain the anomaly. One important example of the limitations in both the

ECCO model and the radar altimetry data types is the lack of coverage in the arctic sea. Mass changes there could have a significant impact on the J_2 variation.

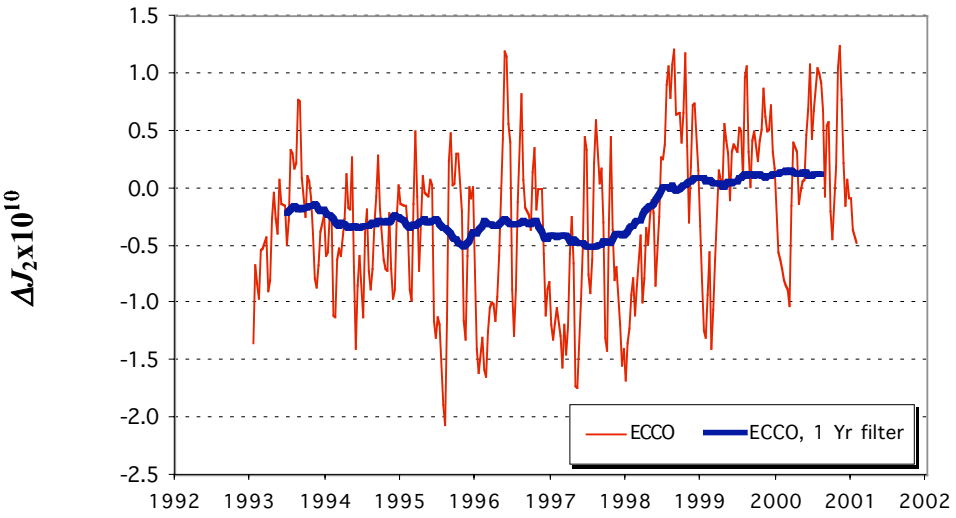

Figure 4. Change in J_2 resulting from ocean mass redistribution in the ECCO assimilation model.

SLR Observation of other Geophysical Signals

The estimated gravity time series also included the non-zonal terms. While expectations were not high for meaningful recovery of these signals, some of the coefficients have shown good correlation with geophysical phenomena. Figure 5 shows the $S_{2,2}$ gravity series with annual signal filtered out. There is a correlation of 0.65 with the Tahiti-Darwin Southern Oscillation Index (SOI), with a twelve-month offset where the gravity signal leads. Also shown is the IB-corrected atmospheric gravity series for the $S_{2,2}$ coefficient. The observed gravity signal is almost an order of magnitude larger than the atmospheric gravity signal, implying that some other process is dominating the observed signal. The correlation to the SOI series is intriguing, especially the twelve-month lead, but it does not constitute proof that a mass transport phenomenon associated with the Southern Oscillation is causing the observation. However, it is suggestive that the gravity data may serve as another useful observation or index. A limitation here are the uncertainties associated with the individual monthly $S_{2,2}$ gravity coefficients, which are about 1.1×10^{-10}. The corresponding uncertainty for an annual value should be about 0.3×10^{-10}. Thus, the observed signal is not very much larger than the uncertainties. More analysis is required to better characterize the observation, and to connect it to the geophysical processes that may be causing it.

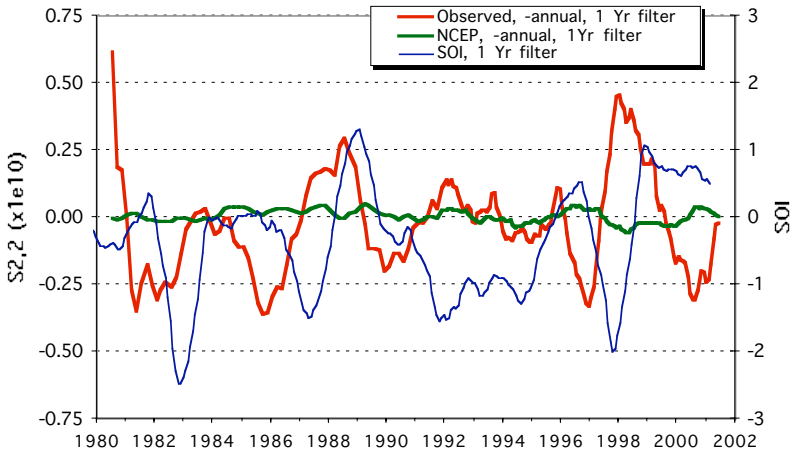

Figure 5. Observed $S_{2,2}$ gravity signal, the Tahiti-Darwin Southern Oscilation Index, and the NCEP derived IB-corrected atmospheric gravity series. All series have had an annual filter applied. The correlation between the SOI series and the observed gravity series is 0.65 when a 12-month shift is applied to the gravity data.

Figure 6 shows the $S_{2,1}$ gravity series, and the corresponding IB-corrected atmospheric gravity series. The long-period differences between the two series corresponds to the differences between the adopted mean $S_{2,1}$ rate (and corresponding polar wander rates) and the IERS annual mean pole variation, so that portion is likely the result of the polar wander. There is a very good agreement with the annual signal from the atmospheric gravity series. This implies that the gravitational signal associated with the atmospheric mass redistribution is being sensed. As with the analysis of the $S_{2,2}$ series, more analysis is required.

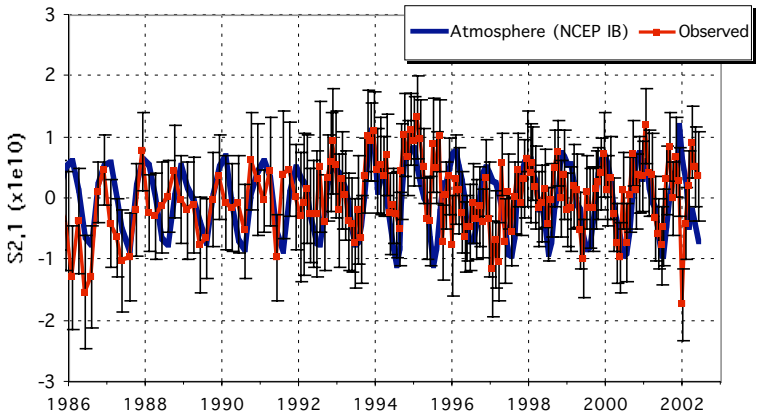

Figure 6. Observed $S_{2,1}$ gravity signal and the NCEP derived IB-corrected atmospheric gravity series. All series have had an annual filter applied.

Conclusions

A large anomaly in J_2 began sometime around 1998, and has persisted until the present time. There are indications that J_2 is returning to the nominal values and long-term trend dictated by post-glacial rebound. Consequently, the deviation may be interannual in nature, and therefore does not necessarily represent a departure from the long-term trend. Ice melting scenarios large enough to explain this deviation produce a large GSL change,

which simply has not been observed. Likewise, the apparent recent turn in J_2 would then imply a recent accumulation of ice mass, which, while not impossible, is unlikely.

There is evidence that some component of the cause of the J_2 anomaly lies within the oceans. The timing corresponds to changes in the primary EOF modes for the SST and SSH in the extra-tropic Pacific regions. The primary SST EOF mode corresponds to PDO, which is generally correlated with the J_2 series. The timing also corresponds to changes in the primary EOF modes of the ECCO model bottom pressure. However, the latter data can only explain about 25% of the observed magnitude of the J_2 change. Nonetheless, the good overall agreement in the timing and nature of the event with the ocean activity warrants more detailed analysis of the ocean's role.

While J_2 analysis results do not conclusively identify the cause of the J_2 anomaly, they do show that a significant geophysical signal has been sensed using SLR. Likewise the $S_{2,1}$ and $S_{2,2}$ gravity signals also show indications of real geophysical signals. The long temporal baseline of the SLR tracking data, and in the recent decade the significant international contributions to the International Laser Ranging Service, make this technology ideal for sensing long-wavelength gravity variations. These observations of changes in the Earth provide a powerful link between models of the hydrosphere, atmosphere, cryosphere and Solid Earth, and can be used as a constraint on the large scale mass transport within the Earth system.

References

Cazenave, A., and R.S. Nerem, Redistributing the Earth's Mass, 297, 783, August 2, 2002.

Chao, B.F., "Anthropogenic impact on global geodynamics due to reservoir water impoundment", *Geophys. Res. Lett.,* 22, 24, 3529-3532, 1995.

Chao, B.F., and W. Kuang, Can the material flow in the fluid core be a source of the observed J2 change? EGS General Assembly, Nice, April, 2002.

Cheng, M.K., et al., "Temporal variations in low degree zonal harmonics from Starlette orbit analysis", *Geophys. Res. Lett.*, 16 (5), 393-396, 1989.

Cheng, M.K., C.K. Shum, and B.D. Tapley, Determination of long-term changes in the Earth's gravity field, *J. Geophys. Res.,* 102, 22377, 1997.

Cox, C.M., S.M. Klosko, and B.F. Chao, Changes in Ice-Mass Balances Inferred From Time Variations of the Geopotential Observed Through SLR and DORIS Tracking, in *Gravity, Geoid and Geodynamics*, M. Sideris ed., IAG Symposia 123 (Springer-Verlag, Heidelberg, 2002).

Cox, C.M., and B.F. Chao, Detection of a Large-Scale Mass Redistribution in the Terrestrial System Since 1998, *Science*, 297, 831, August 2, 2002.

Gegout, P., and A. Cazenave, Temporal Variations of the Earth's Gravity Field for 1985-1989 from LAGEOS, *Geophys. J. Intl.*, 114, 347-359, 1993.

Kuang, W., and B.F. Chao, Geodynamo modeling and core-mantle interactions, in *Earth's Core: Dynamics, Structure, Rotation, Geodynamics Series 31*, Amer. Geophys. Union, Washington DC, 193-212, 2002.

Lemoine, F.G., S.C. Kenyon, J.K. Factor, R.G. Trimmer, N.K. Pavlis, D.S. Chinn, C.M. Cox, S.M. Klosko, S.B. Luthcke, M.H. Torrence, Y.M. Wang, R.G. Williamson, E.C. Pavlis, R.H. Rapp, and T.R. Olson, The Development of the Joint NASA GSFC and the National Imagery and Mapping Agency (NIMA) Geopotential Model EGM96, NASA TR 206861, 1998.

Meier, M., Contribution of small glaciers to global sea level, *Science*, 226,1418-1421, 1984.

Nerem, R.S., and S.M. Klosko, "Secular variations of the zonal harmonics and polar motion as geophysical constraints", in Global Gravity Field and Its Temporal Variations, R. Rapp, A. Cazenave and R. Nerem editors, International Association of Geodesy Symposia 116, Springer Verlag, Berlin-New York, 1996.

Rubincam, D.P., Postglacial Rebound Observed by LAGEOS and the Effective Viscosity of the Lower Mantle, *J. Geophys. Res.,* 89, 1077-1087, 1984.

Schrama, E.J.O., and R.D. Ray, A preliminary tidal analysis of TOPEX/Poseidon altimetry, *J. Geophys. Res*., *99*, 24799–24808, 1994.

Stammer, D., et al., The consortium for estimating the circulation and climate of the ocean (ECCO) -- Science goals and task plan, The ECCO Consortium, Report No.1, November 1999.

Trupin, A., and J. Wahr, "Spectroscopic analysis of global tide gauge sea level data", *Geophys. J. Int.*, 100, 441-453, 1990.

Yoder, C.F., J.G. Williams, J.O. Dickey, B.E. Schutz, R.J. Eanes, and B.D. Tapley, Secular Variation of earth's gravitational harmonic J_2 coefficient from LAGEOS2 and non-tidal acceleration of earth rotation, *Nature*, 303 (5920): 757-762 (1983).

Zwally, J., and A. Brenner, in Altimetry and Earth Science, L.L. Fu, A. Cazenave eds., Academic Press, London, 2001.